

Achievable Rates for Short-Reach Fiber-Optic Channels with Direct Detection

Daniel Plabst, Tobias Prinz, *Student Member, IEEE*, Thomas Wiegart, *Student Member, IEEE*, Talha Rahman, *Member, IEEE*, Nebojša Stojanović, *Member, IEEE*, Stefano Calabrò, Norbert Hanik, *Senior Member, IEEE*, and Gerhard Kramer, *Fellow, IEEE*

Abstract—Spectrally efficient communication is studied for short-reach fiber-optic links with chromatic dispersion (CD) and receivers that employ direction-detection and oversampling. Achievable rates and symbol error probabilities are computed by using auxiliary channels that account for memory in the sampled symbol strings. Real-alphabet bipolar and complex-alphabet symmetric modulations are shown to achieve significant energy gains over classic intensity modulation. Moreover, frequency-domain raised-cosine (FD-RC) pulses outperform time-domain RC (TD-RC) pulses in terms of spectral efficiency for two scenarios. First, if one shares the spectrum with other users then inter-channel interference significantly reduces the TD-RC rates. Second, if there is a transmit filter to avoid interference then the detection complexity of FD-RC and TD-RC pulses is similar but FD-RC achieves higher rates.

Index Terms—Amplitude shift keying, capacity, direct detection, intensity modulation, quadrature amplitude modulation

I. INTRODUCTION

Fiber-optic communication with direct detection (DD) is a cost-effective approach for intra-datacenter communication up to several dozen kilometers [1]. DD receivers measure the amplitude or *intensity* of signals, e.g., by using a photodiode (PD). This reduces the hardware complexity, cost and form factors as compared to coherent receivers [1]–[3]. However, the spectral efficiency (SE) is reduced and compensating transmission impairments is challenging [4]–[6].

DD receivers are usually paired with intensity modulation (IM) transmitters to allow for easy reconstruction of the transmitted data [7]–[9]. More generally, one may use several amplitudes, e.g., Q -PAM with $Q \geq 2$, together with DD and receiver signal processing such as linear equalization and machine learning [6], [10], [11]. IM constellations have a positive mean that aids DD but carries no information and consumes energy.

A. Oversampling

Oversampling at the receiver increases the capacity of DD systems [12]. In fact, if optical amplification (OA) noise is the dominant impairment then DD can operate within 1 bit/s/Hz of the coherent detection capacity, and this motivates using complex-valued constellations [12]–[15]. For example, if the

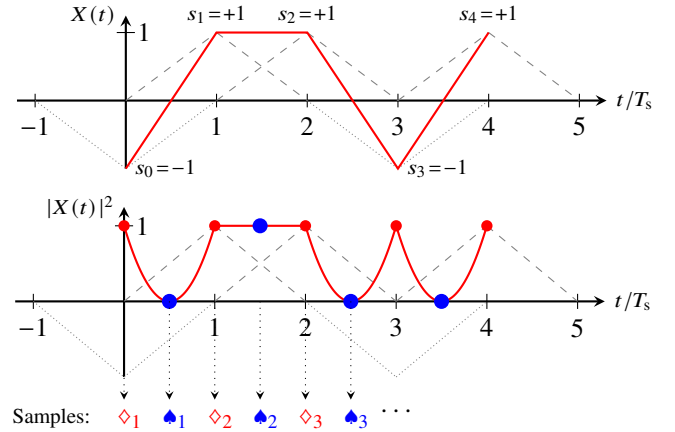


Fig. 1: Phase retrieval in DD.

transmit signal is minimum phase, then its phase can be reconstructed from its intensity by using a Kramers-Kronig (KK) receiver [16]. After recovering the phase, one can mitigate linear impairments such as chromatic dispersion (CD) with standard methods such as linear equalizers or orthogonal frequency division multiplexing (OFDM). However, minimum phase signals require inserting an optical carrier that decreases the SE [13], [17], [18].

Real-valued *bipolar* constellations (Q -ASK) were investigated in [13]. For example, Fig. 1 depicts symbol reconstruction when the baseband pulse is triangular over two symbol periods $2T_s$. The solid curve in the first subplot shows the received baseband signal $X(t)$ when using binary phase-shift keying (BPSK) and the transmit symbol string $(-1, +1, +1, -1, +1)$. The second subplot shows the DD output. Clearly, the samples \diamond_κ at symbol times $t = \kappa T_s$, $\kappa \in \mathbb{Z}$, carry no information. However, the samples \clubsuit_κ at half-symbol times $t = (\kappa + \frac{1}{2})T_s$ experience intersymbol interference (ISI) and give information on phase changes. Thus, one can reconstruct the transmit string by using differential phase decoding [13].

B. Pulse Shaping and Line Coding

The triangular pulse in Fig. 1 was chosen to limit the oversampled ISI but without considering the spectral occupancy. Two classic methods to control the ISI and spectrum, and other signal properties, are *pulse shaping* and *line coding*.

A fundamental approach to pulse shaping with simultaneous timewidth and bandwidth constraints is based on prolate spheroidal wave functions (PSWFs) [19]. The application of PSWFs to data transmission was already pointed out in [20,

Date of current version March 18, 2022.

Accepted to *J. Lightw. Technol.* on January 22, 2022.

D. Plabst, T. Prinz, T. Wiegart, N. Hanik, and G. Kramer are with the Institute for Communications Engineering, Technical University of Munich, 80333 Munich, Germany (e-mail: {daniel.plabst, tobias.prinz, thomas.wiegart, norbert.hanik, gerhard.kramer}@tum.de). T. Rahman, N. Stojanović, and S. Calabrò, are with the Huawei Munich Research Center, 80992 Munich, Germany (e-mail: {talha.rahman, nebojsa.stojanovic, stefano.calabro}@huawei.com).

Sec. 5.2]. In practice, however, one usually uses pulses that satisfy the Nyquist ISI criterion. Perhaps the most popular choice is the class of frequency-domain raised-cosine (FD-RC) functions¹ [21, Eq. (6.17)-(6.18)]. For example, the paper [13] uses an FD-RC pulse with a unit roll-off factor to limit the oversampled ISI to the half-symbol times $t = \pm T_s/2$. However, such pulses are spectrally inefficient. The paper [15] instead uses a time-domain RC (TD-RC) pulse² that extends up to two symbol periods $2T_s$ so that the ISI is limited to the half-symbol times $t = \pm T_s/2$, as in [13] and Fig. 1. We show that the SEs of FD-RC pulses with small roll-off factors are better than those of TD-RC pulses, see Sec. V-C below.

We remark that using TD-RC pulses is a special case of partial-response signaling [23], [24] or faster-than-Nyquist signaling [25]–[27]. Another closely related approach is continuous phase modulation [28], [29]. As pointed out in [30], each of these systems can be understood as a coded modulation where the code simultaneously shapes the signal spectrum and provides coding gain. In the fiber-optic literature, several authors have designed such codes for CD channels and DD receivers. For example, the duobinary signaling of [26] was generalized in [31] and [32] under the names Phase-Shaped Binary Transmission (PSBT) and Phased Amplitude-Shift Signaling (PASS), respectively. These methods were further generalized in [33] and the extensions are called Combined Amplitude-Phase Shift (CAPS) codes in [34], [35].

C. Contributions and Organization

We focus on short-reach fiber-optic channels without OA where thermal noise limits performance [36, p. 154]. Our goal is to study reliable communication for channels with CD, DD and oversampling, and with spectrally efficient pulses. In particular, we focus on FD-RC pulses with small roll-off factor. Such pulses introduce significant ISI when oversampling so that an optimal receiver is complex. However, we find that simplified receivers based on auxiliary (mismatched) channel models can perform well. Moreover, the resulting SEs are benchmarks for designing near-optimal receiver algorithms and for improving signaling.

We remark that many short-reach fiber-optic systems are based on low-cost and low-SE designs with a few wavelengths, short error-control codes, small modulation alphabets, and DD with coarse-quantization and hard-decision decoders. However, the continuing growth in demand for high data rates should result in the usual evolution to systems with high SE via many wavelengths, sophisticated error-control codes, higher-order modulation, and receivers with fine quantization and soft-decision decoders. One purpose of this paper is to study the performance of such systems with one simplifying hardware constraint, namely the use of DD receivers, and with sophisticated signaling and signal processing.

This paper is organized as follows. Sec. II develops continuous- and discrete-time models for short-reach fiber-

optic channels. Sec. III reviews lower and upper bounds on achievable rates based on optimized auxiliary channel densities [37], [38]. Sec. IV reviews symbol-wise maximum *a posteriori* (MAP) detection based on the forward-backward algorithm [39]. Sec. V gives numerical results on the SEs of different constellations, transmit pulses and link lengths. Sec. VI provides concluding remarks and suggests research problems. The Appendix optimizes an auxiliary channel model.

D. Notation

Vectors and matrices are written using bold letters. The transposes of the vector \mathbf{a} is written as \mathbf{a}^T . The $n \times 1$ all-ones and all-zeros vectors are $\mathbf{1}_n$ and $\mathbf{0}_n$, respectively, and the $n \times n$ identity matrix is \mathbf{I}_n . The diagonal matrix with entries taken in order from \mathbf{a} is written as $\text{diag}(\mathbf{a})$. The notation $\mathbf{a} \otimes \mathbf{b}$ refers to the Kronecker product of \mathbf{a} and \mathbf{b} . The determinant and trace of the square matrix \mathbf{A} are written as $\det \mathbf{A}$ and $\text{tr} \mathbf{A}$, respectively. We use the string notation $x_{\kappa}^n = (x_{\kappa}, \dots, x_n)$. Accordingly, we use $\mathbf{x}_{\kappa}^n = (\mathbf{x}_{\kappa}, \dots, \mathbf{x}_n)$ for a string of vectors.

The sinc function is defined as $\text{sinc}(t) = \sin(\pi t)/(\pi t)$. The signal $a(t)$ and its Fourier transform $A(f)$ are related by the notation $a(t) \circ \bullet A(f)$. The expression $g(t) * h(t)$ refers to the convolution of $g(t)$ and $h(t)$ and $\|a(t)\|^2 = \int_{-\infty}^{\infty} |a(t)|^2 dt$ is the energy of $a(t)$.

Random variables (RVs) are written with upper case letters and their realizations with lower-case letters. $\mathbb{E}[\cdot]$ denotes expectation. The mean of the random vector \mathbf{A} is $\boldsymbol{\mu}_{\mathbf{A}} = \mathbb{E}[\mathbf{A}]$ and the covariance matrix of two real random vectors \mathbf{A} , \mathbf{B} is $\mathbf{C}_{\mathbf{AB}} = \mathbb{E}[\mathbf{AB}^T]$. Univariate and multivariate real Gaussian distributions are written as $\mathcal{N}(x; \mu, \sigma^2)$ and $\mathcal{N}(\mathbf{x}; \boldsymbol{\mu}, \mathbf{C})$, respectively, where μ and σ^2 denote mean and variance and $\boldsymbol{\mu}$ and \mathbf{C} denote mean vector and covariance matrix. The distribution or density of the random vector \mathbf{X} is written as $p_{\mathbf{X}}$. The joint distribution or density of \mathbf{X} and \mathbf{Y} is written as $p_{\mathbf{XY}}$. Entropy, divergence and mutual information are defined as in [40]:

$$h(\mathbf{X}) = \mathbb{E} \left[-\log_2 p(\mathbf{X}) \right] \quad (1)$$

$$D(p_{\mathbf{X}} \| p_{\mathbf{Y}}) = \mathbb{E} \left[\log_2 \frac{p_{\mathbf{X}}(\mathbf{X})}{p_{\mathbf{Y}}(\mathbf{X})} \right] \quad (2)$$

$$I(\mathbf{X}; \mathbf{Y}) = D(p_{\mathbf{XY}} \| p_{\mathbf{X}} p_{\mathbf{Y}}) \quad (3)$$

where we measure the quantities in bits. As in (1), we often discard subscripts on distributions or densities if the arguments are uppercase or lowercase versions of their RVs. A basic property of divergence is $D(p_{\mathbf{X}} \| p_{\mathbf{Y}}) \geq 0$ with equality if and only if $p_{\mathbf{X}} = p_{\mathbf{Y}}$ almost everywhere.

II. SYSTEM MODEL

Propagation in fiber is described by the Nonlinear Schrödinger Equation (NLSE) [36, p. 65], [41, Part 2] that exhibits attenuation and CD, both linear effects, and a Kerr nonlinearity. We are interested in short-reach links where the launch power is sufficiently small so that one may neglect the Kerr non-linearity, and where the system is built without OA so that one may neglect optical noise. We next describe the system model in more detail.

¹For memoryless channels one often uses frequency-domain root-raised-cosine pulses with a matched filter so that the end-to-end pulse is FD-RC. However, the CD and DD make this choice less interesting.

²TD-RC pulses are called ‘‘Tukey waveforms’’ in [15] and they have been studied, e.g., for deep-space communication in [22].

A. Continuous-Time Model

The continuous-time model is depicted in Fig. 2, cf. [6].

1) *Transmitter*: Consider a sequence of independent and identically distributed (i.i.d.) symbols $(X_\kappa)_{\kappa \in \mathbb{Z}} = (\dots, X_1, X_2, X_3, \dots)$ with finite alphabet $\mathcal{A} = \{a_1, \dots, a_Q\}$ of cardinality Q and symbol probability mass function (PMF) $p(x) = 1/Q$ for all $x \in \mathcal{A}$. We perform pulse shaping with $g_{\text{tx}}(t)$ to obtain the baseband waveform

$$X(t) = \sum_{\kappa} X_{\kappa} \cdot g_{\text{tx}}(t - \kappa T_s) \quad (4)$$

with symbol-rate $B = 1/T_s$. Common choices for pulse shaping are FD-RC pulses which have the spectrum [21, Eq. (6.17)]

$$G_{\text{tx}}(f) = \begin{cases} 1, & |f| \leq \frac{1-\alpha}{2T_s} \\ \frac{1}{2} \left[1 + \cos \left(\frac{\pi T_s}{\alpha} \left[|f| - \frac{1-\alpha}{2T_s} \right] \right) \right], & \frac{1-\alpha}{2T_s} < |f| \leq \frac{1+\alpha}{2T_s} \\ 0, & \text{otherwise.} \end{cases} \quad (5)$$

We focus mainly on the case $\alpha = 0$ for which we obtain the sinc pulse

$$g_{\text{tx}}(t) = \frac{1}{T_s} \cdot \text{sinc} \left(\frac{t}{T_s} \right) \circ \bullet G_{\text{tx}}(f) = \begin{cases} 1, & |f| \leq \frac{1}{2T_s} \\ 0, & \text{otherwise.} \end{cases} \quad (6)$$

We also consider TD-RC pulses that are time-domain versions of (5), namely

$$g_{\text{tx}}(t) = \begin{cases} 1, & |t| \leq \frac{1-\alpha}{2B} \\ \frac{1}{2} \left[1 + \cos \left(\frac{\pi B}{\alpha} \left[|t| - \frac{1-\alpha}{2B} \right] \right) \right], & \frac{1-\alpha}{2B} < |t| \leq \frac{1+\alpha}{2B} \\ 0, & \text{otherwise.} \end{cases} \quad (7)$$

2) *Fiber-Optic Link*: The channel exhibits CD with response [6, Sec. II.B]

$$h_L(t) \circ \bullet H_L(f) = \exp \left(j \frac{\beta_2}{2} \omega^2 L \right) \quad (8)$$

where β_2 is the CD parameter, $\omega = 2\pi f$ is the angular frequency and L is the fiber length.

3) *Receiver*: The receiver has optical and electrical components. First, a PD outputs the intensity $Z'(t) = |X_L(t)|^2$ of the impinging field [6]. We thus model the PD as having no active bandwidth constraint and we model the PD noise $N'(t)$ in Fig. 2 by a real-valued white Gaussian random process with two-sided power spectral density $N_0/2$.

Next, the receiver has a band-limited sampling device [6, Sec. III.B] with impulse response

$$g_{\text{rx}}(t) = 2B \cdot \text{sinc}(2Bt) \circ \bullet G_{\text{rx}}(f) = \begin{cases} 1, & |f| \leq B \\ 0, & \text{otherwise} \end{cases} \quad (9)$$

that rejects out-of-band noise, avoids aliasing and accommodates the doubled signal bandwidth due to the square-law detector (SLD) operation $|\cdot|^2$. The filtered noise $N(t) = N'(t) * g_{\text{rx}}(t)$ is a zero-mean stationary Gaussian process with autocorrelation function

$$\frac{N_0}{2} \cdot (g_{\text{rx}}(-\tau) * g_{\text{rx}}(\tau)) = \frac{N_0}{2} g_{\text{rx}}(\tau). \quad (10)$$

We similarly define $Z(t) = Z'(t) * g_{\text{rx}}(t)$.

B. Discrete-Time Model

We formulate the discrete-time model for a receiver that samples at rate $1/T'_s = 2B$, i.e., the oversampling factor is $N_{\text{os}} = T_s/T'_s = 2$ samples per transmit symbol³. Let $(X'_k)_{k \in \mathbb{Z}} = ((0, X_\kappa))_{\kappa \in \mathbb{Z}} = (\dots, 0, X_1, 0, X_2, \dots)$ and $Y_k = Y(kT'_s)$, $k \in \mathbb{Z}$, be the upsampled transmitter and receiver sample strings, respectively. The sampler output is

$$Y_k = Z_k + N_k \quad (11)$$

for all k where

$$Z_k = \left(|X_L(t)|^2 * g_{\text{rx}}(t) \right)_{t=kT'_s} \quad (12)$$

and N_1, N_2, \dots is a white Gaussian process with density $p_N(n) = \mathcal{N}(n; 0, \sigma_N^2)$ and $\sigma_N^2 = N_0 B$. Define the combined response of the transmit pulse and fiber as $\psi(t) = g_{\text{tx}}(t) * h_L(t)$ and define the samples $\psi_k = \psi(kT'_s)$, $k \in \mathbb{Z}$. We have $X_L(t) = \sum_{\kappa} X_{\kappa} \cdot \psi(t - \kappa T_s)$ and

$$X_L(kT'_s) = \sum_m X_m \cdot \psi((k-2m)T'_s) = \sum_m \psi_m X'_{k-m}. \quad (13)$$

In the following, we focus on the transmitter pulse shape (6) for which $|X_L(t)|^2 * g_{\text{rx}}(t) = |X_L(t)|^2$ and

$$Z_k = \left| \sum_{m=-\infty}^{\infty} \psi_m X'_{k-m} \right|^2. \quad (14)$$

We convert to vector-matrix notation and collect the upsampled strings for an even number n of time steps:

$$\mathbf{X}' = [0, X_1, 0, X_2, \dots, 0, X_{n/2}]^T \in \mathbb{C}^{n \times 1} \quad (15)$$

$$\mathbf{Z} = [Z_1, Z_2, Z_3, \dots, Z_n]^T \in \mathbb{R}^{n \times 1} \quad (16)$$

$$\mathbf{N} = [N_1, N_2, N_3, \dots, N_n]^T \in \mathbb{R}^{n \times 1} \quad (17)$$

$$\mathbf{Y} = [Y_1, Y_2, Y_3, \dots, Y_n]^T \in \mathbb{R}^{n \times 1}. \quad (18)$$

For illustration, suppose the channel values ψ_m are zero outside the interval $[0, M-1]$ where M is an odd positive integer that represents the oversampled channel memory. Collect these values in the time-reversed vector $\boldsymbol{\psi} = [\psi_{M-1}, \dots, \psi_0]^T$ and define the initial channel state as

$$\mathbf{s}_0 = [0, x_{1-\tilde{M}}, 0, x_{2-\tilde{M}}, \dots, 0, x_0]^T \in \mathbb{C}^{(M-1) \times 1} \quad (19)$$

where $\tilde{M} = (M-1)/2$ is the channel memory in terms of the transmit symbols. The state \mathbf{s}_0 is assumed to be known by the receiver. Define the matrix $\boldsymbol{\Psi} \in \mathbb{C}^{n \times (n+M-1)}$ as the Toeplitz matrix with successively right-shifted versions of $\boldsymbol{\psi}^T$ as its rows. The output of the SLD is

$$\mathbf{Z} = \left| \boldsymbol{\Psi} \begin{bmatrix} \mathbf{s}_0 \\ \mathbf{X}' \end{bmatrix} \right|^2 = |\boldsymbol{\Psi} \tilde{\mathbf{X}}'|^2 \quad (20)$$

where the notation $|\mathbf{X}'|^2$ refers to the vector $[|X'_1|^2, \dots, |X'_n|^2]$, and where $\tilde{\mathbf{X}}' = [\mathbf{s}_0^T, (\mathbf{X}')^T]^T$.

The channel's conditional probability density is Gaussian:

$$p(\mathbf{y}|\mathbf{x}) = \mathcal{N}(\mathbf{y} - |\boldsymbol{\Psi} \tilde{\mathbf{x}}'|^2; \mathbf{0}_n, \sigma_N^2 \mathbf{I}_n). \quad (21)$$

³For a sinc pulse one should oversample at a rate slightly larger than $N_{\text{os}} = 2$ to obtain sufficient statistics. However, we simply use $N_{\text{os}} = 2$. For an FD-RC pulse with positive roll-off factor α the oversampling rate should be at least $N_{\text{os}} = 2(1+\alpha)$ to obtain sufficient statistics.

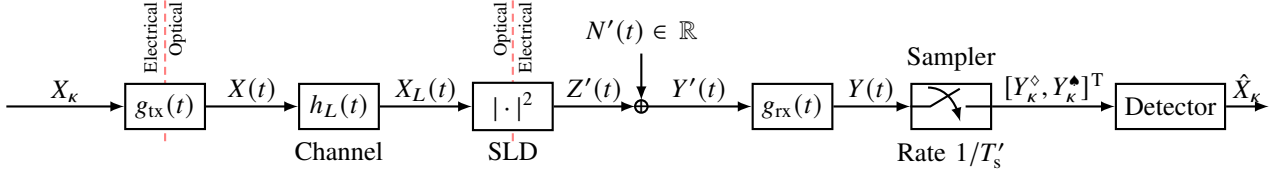
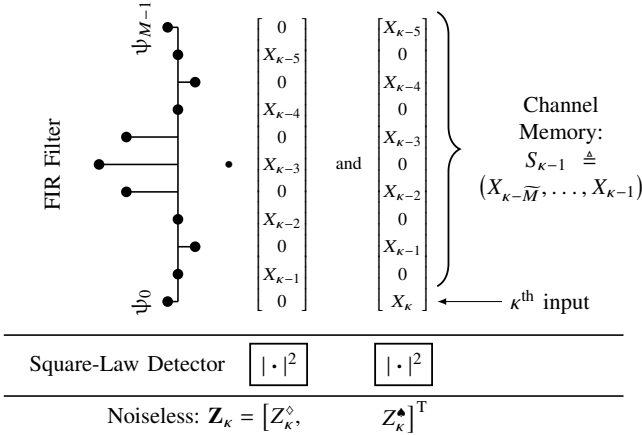


Fig. 2: Communication system with DD.

Fig. 3: Signals for oversampling factor $N_{os} = 2$.

For clarity, we concatenate two subsequent outputs in a vector

$$\mathbf{Z}_\kappa = [Z_\kappa^\diamond, Z_\kappa^\star]^\top. \quad (22)$$

The channel output can similarly be written as

$$\mathbf{Y}_\kappa = [Y_\kappa^\diamond, Y_\kappa^\star]^\top = \mathbf{Z}_\kappa + [N_\kappa^\diamond, N_\kappa^\star]^\top. \quad (23)$$

The convolution and SLD operations are depicted in Fig. 3. Observe that for link length $L = 0$ the Z_κ^\diamond are ISI-free by the choice of $g_{tx}(t)$, while the Z_κ^\star experience ISI.

III. ACHIEVABLE RATES

This section describes how to compute information-theoretic quantities for the underlying ISI channel [42, Sec. II b)]. Define the entropy rate and mutual information rate as the respective

$$h_n(\mathbf{Y}) = \frac{2}{n} h(\mathbf{Y}) \quad (24)$$

$$I_n(\mathbf{X}; \mathbf{Y}) = \frac{2}{n} I(\mathbf{X}; \mathbf{Y}) = h_n(\mathbf{Y}) - h_n(\mathbf{N}). \quad (25)$$

The factor $2/n$ normalizes for the $n/2$ transmit symbols in \mathbf{X} . The rates are thus measured in bits per transmit symbol, also called bits per channel use (bpcu). The limiting rates are

$$h(\mathcal{Y}) = \lim_{n \rightarrow \infty} h_n(\mathbf{Y}), \quad I(\mathcal{X}; \mathcal{Y}) = \lim_{n \rightarrow \infty} I_n(\mathbf{X}; \mathbf{Y}) \quad (26)$$

and these quantities exist if one uses stationary signaling [40, Thm. 4.2.1]. The expression $I(\mathcal{X}; \mathcal{Y})$ in (26) is known to be an achievable rate for reliable communication [43] and one may attempt to maximize $I(\mathcal{X}; \mathcal{Y})$ over all input processes \mathcal{X} to compute the channel capacity. However, the optimization is

usually difficult for nonlinear channels with memory, and for computation and practical implementation one often resorts to i.i.d. signaling. The input process $\mathcal{X} = (X_\kappa)_{\kappa \in \mathbb{Z}}$ is hence stationary and the corresponding output process $\mathcal{Y} = (Y_\kappa)_{\kappa \in \mathbb{Z}}$ is cyclostationary with period N_{os} (for every sample in \mathcal{X} there are two samples in \mathcal{Y}).

A. Computing Entropy and Probabilities

To compute (24), we may use Monte-Carlo simulation to approximate [38]:

$$h_n(\mathbf{Y}) \approx -\frac{2}{n} \log_2 p(\mathbf{y}) \quad (27)$$

where \mathbf{y} is a realization of \mathbf{Y} . The approximation (27) becomes exact in the limit $n \rightarrow \infty$ since \mathcal{Y} is cyclostationary with period N_{os} and ergodic. Define the channel state at time κ as

$$s_{\kappa-1} = (x_{\kappa-M}, \dots, x_{\kappa-1}). \quad (28)$$

The density value $p(\mathbf{y})$ can be computed by marginalizing:

$$p(y_1^n) = \sum_{s_0} \sum_{x_1^{n/2}} p(s_0, x_1^{n/2}, y_1^n) \quad (29)$$

where we use string notation for clarity. We further compute

$$\begin{aligned} p(x_1^{n/2}, y_1^n | s_0) &= \prod_{\kappa=1}^{n/2} p(x_\kappa, \mathbf{y}_\kappa | s_0, x_1^{\kappa-1}) \\ &= \prod_{\kappa=1}^{n/2} p(x_\kappa, \mathbf{y}_\kappa | s_{\kappa-1}) \end{aligned} \quad (30)$$

where we use $\mathbf{Y}_\kappa = (Y_\kappa^\diamond, Y_\kappa^\star)$ and that $(X_\kappa, \mathbf{Y}_\kappa)$ is conditionally independent of $\mathbf{Y}_1^{\kappa-1}$ given $(s_0, X_1^{\kappa-1})$. We thus have

$$p(y_1^n) = \sum_{s_0} \sum_{x_1^{n/2}} p(s_0) \prod_{\kappa=1}^{n/2} p(x_\kappa, \mathbf{y}_\kappa, s_\kappa | s_{\kappa-1}) \quad (31)$$

where s_κ is defined by $(s_{\kappa-1}, x_\kappa)$. Note that $p(x_\kappa, \mathbf{y}_\kappa, s_\kappa | s_{\kappa-1})$ does not depend on the time κ and s_0 is known.

The expression (31) may be further expanded as visualized by the factor graph in Fig. 4: $p(y_1^n)$ can be written as

$$\sum_{s_{n/2}} \sum_{s_{n/2-1}} \cdots \sum_{s_1} \sum_{s_0} \underbrace{p(s_0) \cdot p(x_1, \mathbf{y}_1 | s_1 | s_0) \cdot p(x_2, \mathbf{y}_2 | s_2 | s_1) \cdots}_{\vec{\mu}(s_1)} \cdots \vec{\mu}(s_2) \quad (32)$$

where the state metrics are $\vec{\mu}(s_\kappa) = p(\mathbf{y}_1^\kappa, s_\kappa)$. Eq. (32) is computed on the forward (FW) path of the forward-backward

algorithm [39] through the graph in Fig. 4. We will later also consider the backward (BW) path to compute (33) shown in Fig. 4. The state metrics $\vec{\mu}(s_\kappa)$ quickly approach zero for large κ and we thus normalize as in [38]. Next, decompose

$$p(x_\kappa, \mathbf{y}_\kappa, s_\kappa | s_{\kappa-1}) = \underbrace{p(\mathbf{y}_\kappa | x_\kappa, s_{\kappa-1})}_{(a)} \underbrace{p(s_\kappa | x_\kappa, s_{\kappa-1})}_{(b)} \underbrace{p(x_\kappa | s_{\kappa-1})}_{(c)} \quad (34)$$

where the term (a) is

$$p(\mathbf{y}_\kappa | x_\kappa, s_{\kappa-1}) = p(y_\kappa^\diamond | s_{\kappa-1}) \cdot p(y_\kappa^\spadesuit | x_\kappa, s_{\kappa-1}) \quad (35)$$

and where

$$p(y_\kappa^\diamond | s_{\kappa-1}) = p_N(y_\kappa^\diamond - |[0, x_{\kappa-\tilde{M}}, 0, \dots, x_{\kappa-1}, 0] \cdot \boldsymbol{\Psi}|^2) \quad (36)$$

$$p(y_\kappa^\spadesuit | x_\kappa, s_{\kappa-1}) = p_N(y_\kappa^\spadesuit - |[x_{\kappa-\tilde{M}}, \dots, x_{\kappa-1}, 0, x_\kappa] \cdot \boldsymbol{\Psi}|^2). \quad (37)$$

The term (b) in (34) is 1 if, given $X_\kappa = x_\kappa$, there is a state transition $s_{\kappa-1} \rightarrow s_\kappa$ and is 0 otherwise. Since we use i.i.d. signaling, the term (c) is

$$p(x_\kappa | s_{\kappa-1}) = p(x_\kappa). \quad (38)$$

B. Auxiliary Channel and Mutual Information Rates

The complexity of computing $h_n(\mathbf{Y})$ grows with the number of states, which in turn grows exponentially in the memory length \tilde{M} . To limit receiver complexity, we must usually use a much smaller number \tilde{N} of taps, see Fig. 5.

Consider the Gaussian auxiliary channel with mean $\boldsymbol{\mu}_Q$ and covariance matrix \mathbf{C}_{QQ} :

$$q(\mathbf{y}|\mathbf{x}) = \mathcal{N}(\mathbf{y} - |\boldsymbol{\Psi}'\tilde{\mathbf{x}}'|^{o2}; \boldsymbol{\mu}_Q, \mathbf{C}_{QQ}) \quad (39)$$

where $\boldsymbol{\Psi}'$ is a Toeplitz channel matrix that has entries corresponding to a time-reversed channel $\boldsymbol{\psi}' = [\psi_{N-1}, \dots, \psi_0]^T$ with memory $\tilde{N} = (N-1)/2$ rather than the channel $\boldsymbol{\psi} = [\psi_{M-1}, \dots, \psi_0]^T$ that has memory $\tilde{M} = (M-1)/2$. The corresponding channel output density is

$$q(\mathbf{y}) = \sum_{\mathbf{x}} p(\mathbf{x}) \cdot q(\mathbf{y}|\mathbf{x}) \quad (40)$$

and we define the ‘‘reverse’’ channel as

$$r(\mathbf{x}|\mathbf{y}) = \frac{p(\mathbf{x}) \cdot q(\mathbf{y}|\mathbf{x})}{q(\mathbf{y})}. \quad (41)$$

We now follow the steps in [38, p. 3503] and write

$$I_n(\mathbf{X}; \mathbf{Y}) = I_{q,n}(\mathbf{X}; \mathbf{Y}) + \frac{2}{n} D(p_{\mathbf{X}\mathbf{Y}} \| p_{\mathbf{Y}} \cdot r_{\mathbf{X}|\mathbf{Y}}) \quad (42)$$

where

$$I_{q,n}(\mathbf{X}; \mathbf{Y}) = \frac{2}{n} \mathbb{E} \left[\log_2 \frac{q(\mathbf{Y}|\mathbf{X})}{q(\mathbf{Y})} \right] \quad (43)$$

and where the expectation is with respect to (w.r.t.) $p(\mathbf{x}, \mathbf{y})$. The limiting rate is (see (26))

$$I_q(\mathcal{X}; \mathcal{Y}) = \lim_{n \rightarrow \infty} I_{q,n}(\mathbf{X}; \mathbf{Y}) \quad (44)$$

and this quantity exists [40, Thm. 4.2.1] if one uses stationary signaling. Since (26) is an achievable rate for reliable communication, so is the rate (44) by using (42). The expression $I_{q,n}(\mathbf{X}; \mathbf{Y})$ can be approximated via simulation as

$$I_{q,n}(\mathbf{X}; \mathbf{Y}) \approx \frac{2}{n} \log_2 \frac{q(\mathbf{y}|\mathbf{x})}{q(\mathbf{y})} \quad (45)$$

where \mathbf{x} and \mathbf{y} are realizations of \mathbf{X} and \mathbf{Y} , respectively. The approximation becomes exact in the limit $n \rightarrow \infty$ since \mathcal{X} is stationary and \mathcal{Y} is cyclostationary with period N_{os} , and both processes are ergodic.

C. Computing Achievable Rates

We use the auxiliary channel (39) with reduced memory \tilde{N} to simplify computation. Given \tilde{N} , we seek the $\boldsymbol{\mu}_Q$ and the diagonal \mathbf{C}_{QQ} that maximize $I_{q,n}(\mathbf{X}; \mathbf{Y})$, which is equivalent to minimizing the divergence in (42) for large n . Expanding this divergence, we have

$$\begin{aligned} D(p_{\mathbf{X}\mathbf{Y}} \| p_{\mathbf{Y}} \cdot r_{\mathbf{X}|\mathbf{Y}}) \\ = D(p_{\mathbf{X}\mathbf{Y}} \| p_{\mathbf{X}} \cdot q_{\mathbf{Y}|\mathbf{X}}) - D(p_{\mathbf{Y}} \| q_{\mathbf{Y}}) \geq 0. \end{aligned} \quad (46)$$

Minimizing $D(p_{\mathbf{X}\mathbf{Y}} \| p_{\mathbf{X}} \cdot q_{\mathbf{Y}|\mathbf{X}})$ thus makes both the divergences $D(p_{\mathbf{X}\mathbf{Y}} \| p_{\mathbf{Y}} \cdot r_{\mathbf{X}|\mathbf{Y}})$ and $D(p_{\mathbf{Y}} \| q_{\mathbf{Y}})$ small, and serves as a proxy for finding good $\boldsymbol{\mu}_Q$ and diagonal \mathbf{C}_{QQ} . The Appendix formulates an optimization problem for this proxy and provides the solution for $\boldsymbol{\mu}_Q$ and general \mathbf{C}_{QQ} . We will consider *independent* noise that is identically distributed on the \diamond -samples, and identically distributed on the \spadesuit -samples. The mean and covariance matrix thus have the form $\boldsymbol{\mu}_Q = ([1, \dots, 1] \otimes [\mu_1, \mu_2])^T$ and $\mathbf{C}_{QQ} = \text{diag}([1, \dots, 1] \otimes [\sigma_{N1}^2, \sigma_{N2}^2])$, respectively, where $\mu_1, \mu_2, \sigma_{N1}^2, \sigma_{N2}^2$ can be computed analytically or estimated via Monte Carlo simulation.

We will also be interested in the individual contributions of the \mathbf{Y}^\diamond and \mathbf{Y}^\spadesuit samples to the achievable rates. To compute these, consider the chain rule for mutual information:

$$I_{q,n}(\mathbf{X}; \mathbf{Y}) = I_{q,n}(\mathbf{X}; \mathbf{Y}^\diamond) + I_{q,n}(\mathbf{X}; \mathbf{Y}^\spadesuit | \mathbf{Y}^\diamond). \quad (47)$$

We compute $I_{q,n}(\mathbf{X}; \mathbf{Y})$ via (45) and by using the FW path of the graph in Fig. 4 for the auxiliary channel $q(\mathbf{y}|\mathbf{x})$ and input distribution $p(\mathbf{x})$. The term $I_{q,n}(\mathbf{X}; \mathbf{Y}^\diamond)$ is the usual IM-DD rate with Nyquist-rate sampling that can be found by numerical integration, e.g., Gauss-Hermite quadrature algorithms [44, A.3]. The final term $I_{q,n}(\mathbf{X}; \mathbf{Y}^\spadesuit | \mathbf{Y}^\diamond)$ is now obtained by (47). The limiting versions of the individual expressions are

$$I_q(\mathcal{X}; \mathcal{Y}^\diamond) = \lim_{n \rightarrow \infty} I_{q,n}(\mathbf{X}; \mathbf{Y}^\diamond) \quad (48)$$

$$I_q(\mathcal{X}; \mathcal{Y}^\spadesuit | \mathcal{Y}^\diamond) = \lim_{n \rightarrow \infty} I_{q,n}(\mathbf{X}; \mathbf{Y}^\spadesuit | \mathbf{Y}^\diamond) \quad (49)$$

which exist for stationary signaling.

D. Upper Bounds on Mutual Information

An *upper* bound on mutual information is [37]:

$$\begin{aligned} I(\mathbf{X}; \mathbf{Y}) &= D(p_{\mathbf{Y}|\mathbf{X}} \| w_{\mathbf{Y}} | p_{\mathbf{X}}) - D(p_{\mathbf{Y}} \| w_{\mathbf{Y}}) \\ &\leq D(p_{\mathbf{Y}|\mathbf{X}} \| w_{\mathbf{Y}} | p_{\mathbf{X}}) \end{aligned} \quad (50)$$

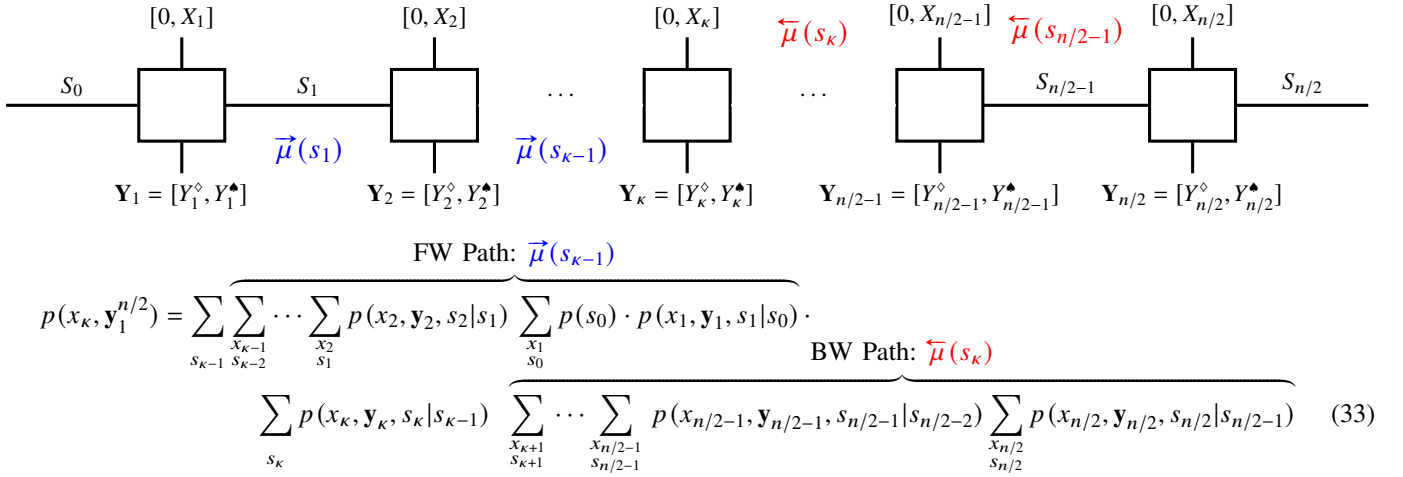


Fig. 4: Factor graph and associated computation for the FW and BW paths with two-fold oversampling.

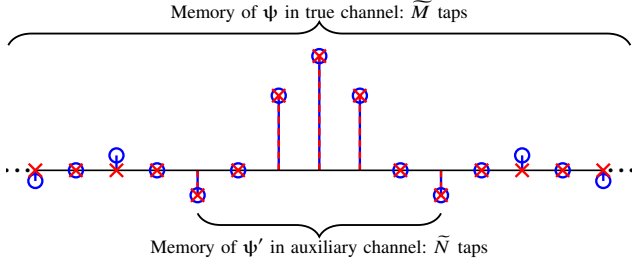


Fig. 5: Memory comparison of true and auxiliary channels.

where $w(\mathbf{y})$ is any output density and $p(\mathbf{y})$ is absolutely continuous w.r.t. $w(\mathbf{y})$. For simplicity, we choose

$$w(\mathbf{y}) = \mathcal{N}(\mathbf{y}; \boldsymbol{\mu}_Y, \mathbf{C}_{YY}). \quad (51)$$

Using $\mathbf{C}_{YY} = \mathbf{C}_{ZZ} + \sigma_N^2 \mathbf{I}_n$, the bound (50) is

$$I(\mathbf{X}; \mathbf{Y}) \leq \frac{1}{2} \log_2 \det \left(\mathbf{I}_n + \frac{\mathbf{C}_{ZZ}}{\sigma_N^2} \right) \quad (52)$$

where we applied standard identities [40, Ch. 8]. Intuitively, the Gaussian density (51) is a good choice at low Signal-to-Noise Ratio (SNR) where the AWGN dominates the SLD output. At high SNR, however, a Gaussian density fails to accurately model the SLD output.

A simpler upper bound follows by the Hadamard [40, Eq. (8.64)] and Jensen inequalities [40, Eq. (2.75)]:

$$\frac{1}{2} \log_2 \det \left(\mathbf{I}_n + \frac{\mathbf{C}_{ZZ}}{\sigma_N^2} \right) \leq \frac{n}{2} \log_2 \left(1 + \frac{\bar{\sigma}_Z^2}{\sigma_N^2} \right) \quad (53)$$

where $\bar{\sigma}_Z^2 = \frac{1}{n} \text{tr} \mathbf{C}_{ZZ}$. An expression for \mathbf{C}_{ZZ} for real-valued i.i.d. inputs that have symmetries is derived in [6, Eq. (23)]. For other input distributions, \mathbf{C}_{ZZ} can be found by Monte-Carlo simulation. We remark that the bounds (52) and (53) depend on the pulse shape and higher-order moments of the transmit symbols \mathbf{X} due to the SLD [6, Eq. (23)].

IV. SYMBOL-WISE MAP DETECTION

In addition to computing achievable rates, we study decoding with the symbol *a posteriori* probabilities (APPs) $p(x_k | \mathbf{y}_1^{n/2})$. We have $p(x_k | \mathbf{y}_1^{n/2}) \propto p(x_k, \mathbf{y}_1^{n/2})$ because $p(\mathbf{y}_1^{n/2})$ is a constant w.r.t. the decisions. Taking a hard decision (HD) based on the APP gives the MAP symbol estimates

$$\hat{x}_k = \arg \max_{x_k} p(x_k, \mathbf{y}_1^{n/2}) \quad (54)$$

where

$$p(x_k, \mathbf{y}_1^{n/2}) = \sum_{s_0} \sum_{x_1^{n/2} \setminus x_k} p(s_0, x_1^{n/2}, \mathbf{y}_1^{n/2}) \quad (55)$$

and $\sum_{x_1^{n/2} \setminus x_k} f(x_1^{n/2})$ denotes a sum over all strings $x_1^{n/2}$ but where the k^{th} entry of the strings remains fixed.

The value (55) can be efficiently computed for finite state channels using the forward-backward algorithm, as depicted in Fig. 4 and (33). The BW path metrics are defined as

$$\overleftarrow{\mu}(s_k) = p(\mathbf{y}_{k+1}^{n/2} | s_k). \quad (56)$$

The FW and BW path recursions thus read:

$$\begin{aligned} \text{FW:} \quad \vec{\mu}(s_k) &= \sum_{x_k, s_{k-1}} p(x_k, \mathbf{y}_k, s_k | s_{k-1}) \cdot \vec{\mu}(s_{k-1}) \\ \text{BW:} \quad \overleftarrow{\mu}(s_{k-1}) &= \sum_{x_k, s_k} p(x_k, \mathbf{y}_k, s_k | s_{k-1}) \cdot \overleftarrow{\mu}(s_k) \end{aligned} \quad (57)$$

where $\kappa \in \{1, \dots, n/2\}$, $\vec{\mu}(s_0) = p(s_0)$ and $\overleftarrow{\mu}(s_{n/2}) = p(s_{n/2})$. We again normalize the FW and BW path metrics for every iteration to avoid numerical issues. The APPs can also be computed for the auxiliary channel (39) rather than the true channel.

The SLD causes phase ambiguities in MAP detection for certain modulation alphabets with i.i.d. encoding [45]–[47]. These ambiguities can be avoided by differential encoding [13], [48]–[51] or other precoders. We use differential encoding for the transmit symbol phases and include decoding in the forward-backward algorithm at the receiver.

V. SIMULATION RESULTS AND DISCUSSION

We compute achievable rates and error probabilities for a standard single-mode fiber (SSMF) at wavelength 1550 nm with $\beta_2 = -2.168 \times 10^{-23} \text{ s}^2/\text{km}$, attenuation factor 0.2 dB/km, link lengths $L = 0$ and $L = 30$ km, receiver oversampling rate $N_{\text{os}} = 2$ and symbol rate $B = 35$ GBaud. We use single-polarization transmission and neglect the Kerr nonlinearity. The transmit blocks have at least $n/2 = 20 \times 10^3$ symbols for all plots. The average transmit power is

$$P_{\text{tx}} = \frac{\mathbb{E} [\|X(t)\|^2]}{(n/2)T_s} \quad (58)$$

and the noise variance is $\sigma_N^2 = 1$ so that $\text{SNR} = P_{\text{tx}}$.

The constellations have one of $Q = 2, 4, 8$. The PAM and ASK constellations have equidistant spacing for the X_κ , e.g., the 4-PAM and 4-ASK alphabets are $\mathcal{A} = \{0, 1, 2, 3\}$ and $\mathcal{A} = \{-3, -1, 1, 3\}$, respectively. This means that the alphabets for the $|X_\kappa|^2$ after the SLD are $\{0, 1, 4, 9\}$ and $\{1, 9\}$, respectively. We remark that these constellations implement *geometric shaping* after the SLD that is beneficial at intermediate SNRs. One could, of course, optimize the spacing for each SNR and this is interesting future work. We also consider quadrature amplitude modulation (QAM) with $Q = 4$ (QPSK) and $\mathcal{A} = \{\pm 1, \pm j\}$, as well as the 2-ring/4-ary alphabet $\mathcal{A} = \{\pm 1, \pm j, \pm 2, \pm 2j\}$, denoted as 8-Star-QAM (SQAM). The corresponding $|X_\kappa|^2$ alphabets are $\{1\}$ and $\{1, 4\}$, respectively. We use differential phase encoding for all constellations.

The FD-RC pulses have small roll-off factors $\alpha = 0$ (sinc pulse) and $\alpha = 0.2$, while the TD-RC pulse [15, Eq. (2)] has a large roll-off factor $\alpha = 0.9$. The SE of FD-RC is

$$\text{SE} = \frac{R}{(1 + \alpha) \cdot B \cdot T_s} \quad [\text{bit/s/Hz}]. \quad (59)$$

For TD-RC, we measure the bandwidth as the smallest frequency range with 95% of the transmit power. This bandwidth turns out to be 15% larger than the corresponding sinc pulse, see [15, Table I].

We remark that the expression (14) changes for FD-RC pulses with positive roll-off factor and for TD-RC pulses because the bandwidth of $Z'(t)$ is larger than $2B$. The receiver filter $g_{\text{rx}}(t)$ thus cuts off part of the spectrum. We simulated the system with oversampling factor $N_{\text{sim}} = 4$ and then downsampled to $N_{\text{os}} = 2$. The result is

$$Z_k = \sum_{\ell=-\infty}^{\infty} g_{\text{rx}}(\ell T'_s) \left| \sum_{m=-\infty}^{\infty} \psi_m X'_{(d \cdot k - \ell) - m} \right|^2 \quad (60)$$

where $\psi_m = \psi(mT'_s)$ and the N_{sim} -fold upsampled string is $(X'_m)_{m \in \mathbb{Z}} = ((0, 0, 0, X_\kappa))_{\kappa \in \mathbb{Z}}$ with the sampling time $T'_s = T_s/N_{\text{sim}}$ and with $d = N_{\text{sim}}/N_{\text{os}}$.

A. $L = 0$ Rates

Fig. 6 plots the rates (45), upper bounds (52), and HD symbol error rates (SERs) for a sinc pulse and $L = 0$. Within the subplots, we vary the memory \tilde{N} of the auxiliary channel. We remark that the simulation complexity grows rapidly with Q and \tilde{N} so that we had to use a smaller \tilde{N} for larger Q .

Subplots (a)-(b) show that ASK and QAM benefit considerably from increased \tilde{N} because the phase transitions must

be recovered from the \spadesuit -samples that experience significant ISI. PAM is less sensitive to model mismatch and subplot (a) suggests that 2-PAM should be preferred over 2-ASK. However, from subplot (d) we see that the bipolar 4-ASK and 8-ASK alphabets gain approximately 0.4 dB and 0.9 dB over 4-PAM and 8-PAM, respectively, at intermediate SNRs.

Subplot (e) shows (45) for 8-PAM/ASK/SQAM as well as the information in the \spadesuit -samples given the \diamond -samples. As expected, $I_q(X; \mathcal{Y}^\spadesuit | \mathcal{Y}^\diamond)$ for 8-PAM approaches zero at high SNR because the \diamond -samples suffice to reconstruct the transmitted symbols. However, the \spadesuit -samples are useful at intermediate SNRs. For 8-ASK and 8-SQAM, the \spadesuit -samples contribute approximately 0.5 bpcu and 1 bpcu, respectively, at high SNR. One would expect the phase modulations to give 1 bpcu and 2 bpcu, respectively, which shows that there are substantial losses due to the auxiliary channel mismatch.

Observe that the upper bounds are tight at low SNR and loose at high SNR. The upper bounds for 4-QAM and 8-SQAM are lower than for Q -ASK. The information in the \diamond -samples is zero for 4-QAM.

Finally, subplot (f) depicts the uncoded HD SERs with MAP decisions. The SERs of PAM decrease with SNR whereas the SERs of ASK and (S)QAM saturate due to the auxiliary channel mismatch. Moreover, (S)QAM with a sinc filter exhibits phase ambiguities despite differential encoding at the transmitter, and this causes an error floor.

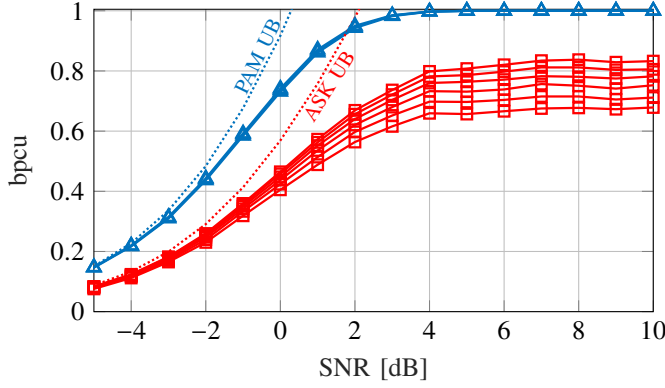
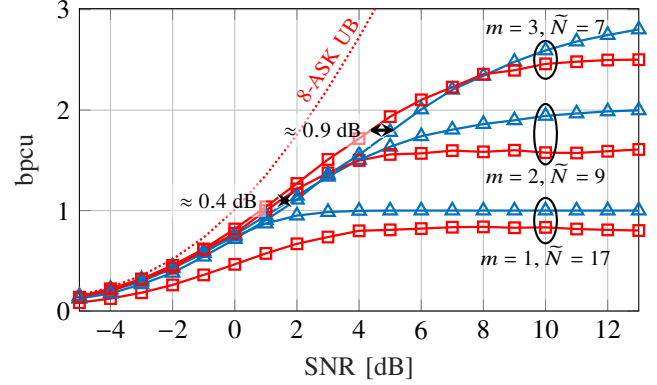
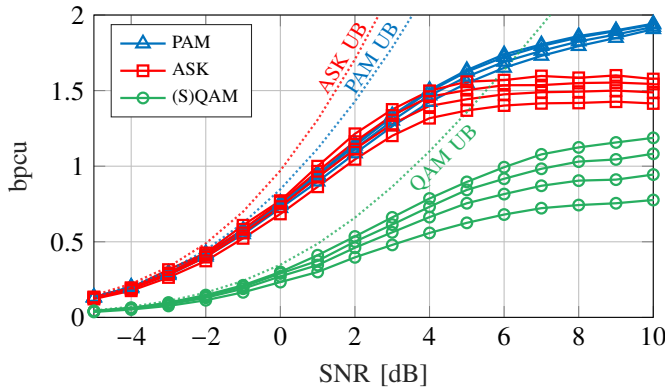
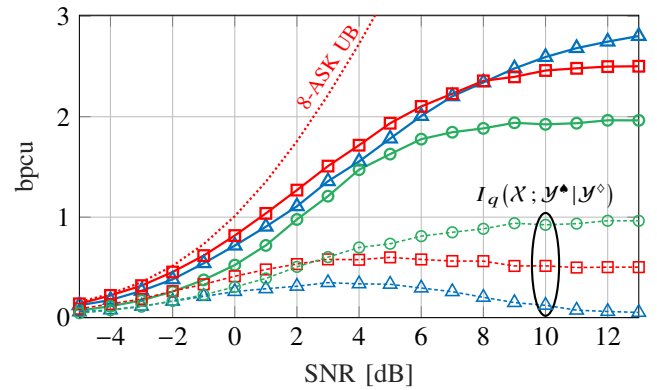
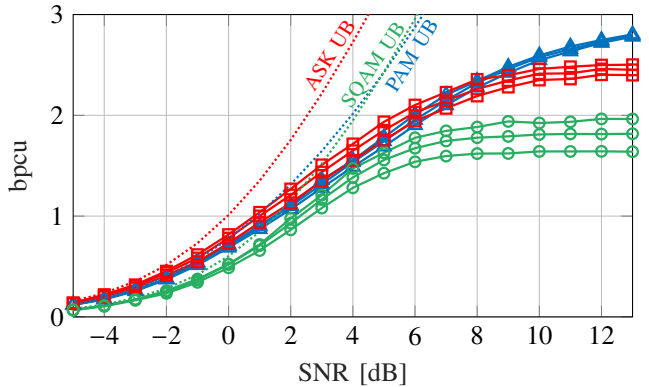
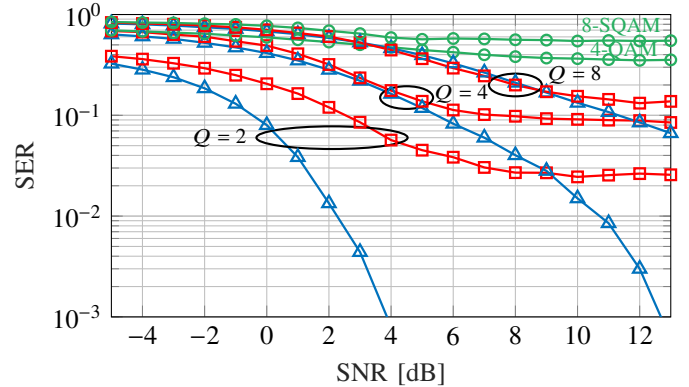
Fig. 7 plots the $L = 0$ rates (44), (48) and (49) with oversampling, Nyquist-rate sampling and conditional mutual information, respectively, for $Q = 8$ and the largest studied auxiliary memory. Observe that there is considerable information in the \spadesuit -samples. As expected, $I_q(X; \mathcal{Y}^\diamond)$ saturates at the logarithm of the number of intensities of the modulation, i.e., 3, 2, 1 bits for 8-PAM, 8-ASK, 8-SQAM, respectively.

B. CD Rates

The next plots show that CD inherently resolves phase ambiguities. The reason is that CD spreads symbols over multiple receive samples, and consequently the \diamond -samples have both intensity and phase information when using bipolar and complex alphabets. CD can thus be interpreted as a precoding for the receiver, i.e., even for short link lengths near $L = 0$ one can avoid phase ambiguities by appropriate precoding.

Fig. 8 shows rate bounds for a sinc pulse and a link with $L = 30$ km that has 6 dB of attenuation. The first and second columns are for $Q = 4$ and $Q = 8$, respectively. The first column shows that 4-ASK and 4-QAM perform equally well, achieve the maximal $\log_2 Q = 2$ bits at high SNR and gain approximately 1.4 dB over 4-PAM. The SER plot (c) shows that differential coding gives a waterfall behaviour for ASK and QAM (here QPSK). The plots in the second column show similar behaviour for $Q = 8$, where 8-ASK (a bipolar constellation) and 8-SQAM (a complex-alphabet constellation) gain approximately 1.5 dB and 1.8 dB over PAM, respectively. The achievable rates for both modulation formats saturate due to the auxiliary model mismatch. The resulting uncoded HD SERs decay slowly and eventually saturate.

To reduce the model mismatch, we replace the sinc pulse by an FD-RC pulse with roll-off factor $\alpha = 0.2$. The maximum

(a) 2-PAM/ASK, $\tilde{N} = [7, 9, 11, 13, 15, 17]$.(d) Q -PAM/ASK for the largest \tilde{N} studied here.(b) 4-PAM/ASK/QAM, $\tilde{N} = [3, 5, 7, 9]$.(e) 8-PAM/ASK/SQAM for the largest studied \tilde{N} and conditional information rate (49) (dotted with marks).(c) 8-PAM/ASK/SQAM, $\tilde{N} = [3, 5, 7]$.(f) Uncoded HD SERs of Q -PAM/ASK/SQAM according to (a)-(c) for largest studied \tilde{N} .Fig. 6: Achievable rates, upper bounds and HD SERs for $L = 0$. The colors in subplot (b) are used for all plots in the figure.

SE is thus reduced by a factor of $5/6$. The remaining system is described in Fig. 2. The SLD again doubles the bandwidth and the excess bandwidth is removed by the antialiasing filter $g_{rx}(t)$ in (12). Fig. 9 plots the SEs for $Q = 8$. Observe that at high SNR the SEs for all constellations are closer to the maximum SE (here 2.5 bit/s/Hz) as compared to Fig. 6. For SEs near 2 bit/s/Hz and $L = 0$, 8-ASK gains approximately 1.7 dB over 8-PAM, whereas 8-SQAM and 8-ASK perform equally well. For SEs near 2 bit/s/Hz and $L = 30 \text{ km}$, 8-

SQAM and 8-ASK gain approximately 3 dB and 2.1 dB over 8-PAM, respectively.

C. Comparison of sinc and TD-RC Pulses for $L = 0$

TD-RC pulses are shorter than FD-RC pulses and this reduces the detection complexity when using a receiver filter

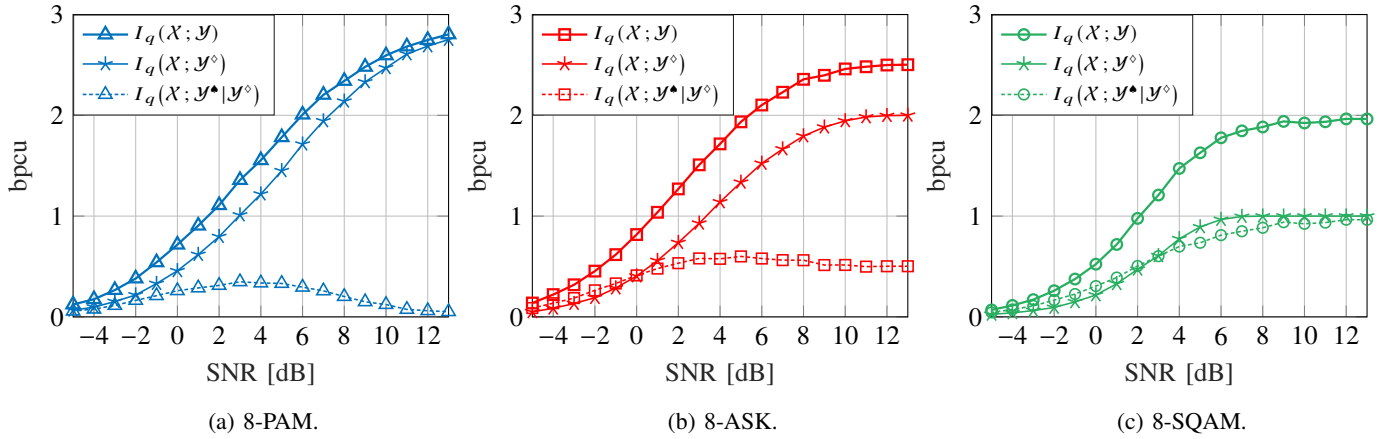


Fig. 7: Achievable rates for $L = 0$, $Q = 8$, and $\tilde{N} = 7$.

with finite time duration⁴. On the other hand, TD-RC leaks energy outside the FD-RC frequency band and this causes interference to neighboring bands and also distortions with devices that have limited bandwidth.

We consider two scenarios to compare the schemes, see Fig. 10. First, the case where one uses wavelength division multiplexing (WDM) to share the spectrum. We consider two neighbouring WDM channels centered at $\pm B_c$ from the channel of interest, see Fig. 10 (a). TD-RC signals thus cause inter-channel interference (ICI) because their spectrum has infinite support. Second, the case where one uses an additional sinc pulse filter $g_c(t)$ with bandwidth B_c at the transmitter to avoid ICI, see Fig. 10 (b) where the new transmit filter is $g_{tx}(t) * g_c(t)$. For both cases, the filter $g_c(t)$ is also placed before the SLD to select the center channel, and there is an antialiasing filter $g_{rx}(t)$ of bandwidth $2B$ after the SLD, see (9). The receiver oversampling rate is $N_{os} = 2$.

Fig. 11 compares the performance for $L = 0$, $Q = 8$, the sinc pulse (6) and the TD-RC pulse with roll-off factor $\alpha = 0.9$. For the latter pulse, the filter $g_{rx}(t)$ passes 99% of the energy of $Z'(t)$. The filters $g_c(t)$ and $g_{rx}(t)$ cause additional ISI so we set the maximal detector memory to $\tilde{N} = 7$ for both pulses. Fig. 11 shows that ICI reduces the SE of TD-RC. Sinc pulses gain 2.4 dB and 3.5 dB over TD-RC with ICI for 8-PAM and 8-ASK, respectively, when operating at a SE of approximately 1.9 bit/s/Hz. The gain is 3 dB for 8-SQAM when operating at a SE of approximately 1.6 bit/s/Hz.

To avoid or limit ICI, we choose $B_c = B$ for the sinc pulse and $B_c = 1.15B$ for the TD-RC pulse and the transmit filter $g_c(t)$. Fig. 11 shows that the sinc pulse has better SEs for PAM and ASK, and these two constellations have higher rates than SQAM. Sinc pulses gain 1.2 dB and 0.4 dB over TD-RC for 8-PAM and 8-ASK, respectively, when operating at a SE of approximately 1.9 bit/s/Hz. For 8-SQAM and SEs near 1.4 bit/s/Hz, sinc pulses gain 0.7 dB over TD-RC. At high-

SNR, the TD-RC pulse outperforms the sinc pulse because of the auxiliary model mismatch.

Fig. 11 also shows the SEs if the receiver uses a lower-complexity forward-backward algorithm with $\tilde{N} = 3$. For 8-PAM, the sinc pulse outperforms the TD-RC pulse for all SNRs. For 8-ASK, the two schemes perform almost the same. For 8-SQAM, one might prefer the TD-RC pulse because it has a smaller auxiliary model mismatch. However, we expect that the sinc pulse has more potential if one can find low-complexity detection algorithms that perform almost as well as the forward-backward algorithm.

VI. CONCLUSIONS

We investigated spectrally efficient communication for short-reach fiber-optic links with DD. CD mitigates DD phase ambiguities by distributing the amplitude and phase information onto receiver samples at both symbol- and half-symbol times. This increases the achievable rates and reduces error propagation for symbol-wise MAP estimation. FD-RC pulses outperform TD-RC pulses in terms of SE.

There are many questions to explore. For example, one could design precoders to increase rates via higher-order complex-valued modulation formats. One can further remove sequences that cause phase ambiguities [15] and this approach can readily be integrated in forward-backward processing. Next, one might consider pulse shaping with PSWFs that are band-limited and have the maximum energy in a given time interval, a property that should decrease the auxiliary model mismatch for a fixed memory \tilde{N} . The design of complex-valued pulse shapes [12] can increase the number of distinct receiver strings and thereby the achievable rates. One can also optimize the achievable rates via geometric and/or probabilistic shaping of the constellation points. Finally, one can design codes and simplified detection and decoding algorithms.

ACKNOWLEDGMENT

The authors wish to thank F. J. García-Gómez and the reviewers for useful suggestions.

⁴The paper [15] uses an integrate-and-dump filter. An optimal detector instead projects $Y'(t)$ in Fig. 2 onto the space spanned by all possible signals $Z'(t)$. For example, for FD-RC pulses one may project onto the space spanned by the sinc pulses $B_\alpha \text{sinc}(B_\alpha t - \kappa)$ where $B_\alpha = 2B(1 + \alpha)$ and $\kappa \in \mathbb{Z}$, see (9).

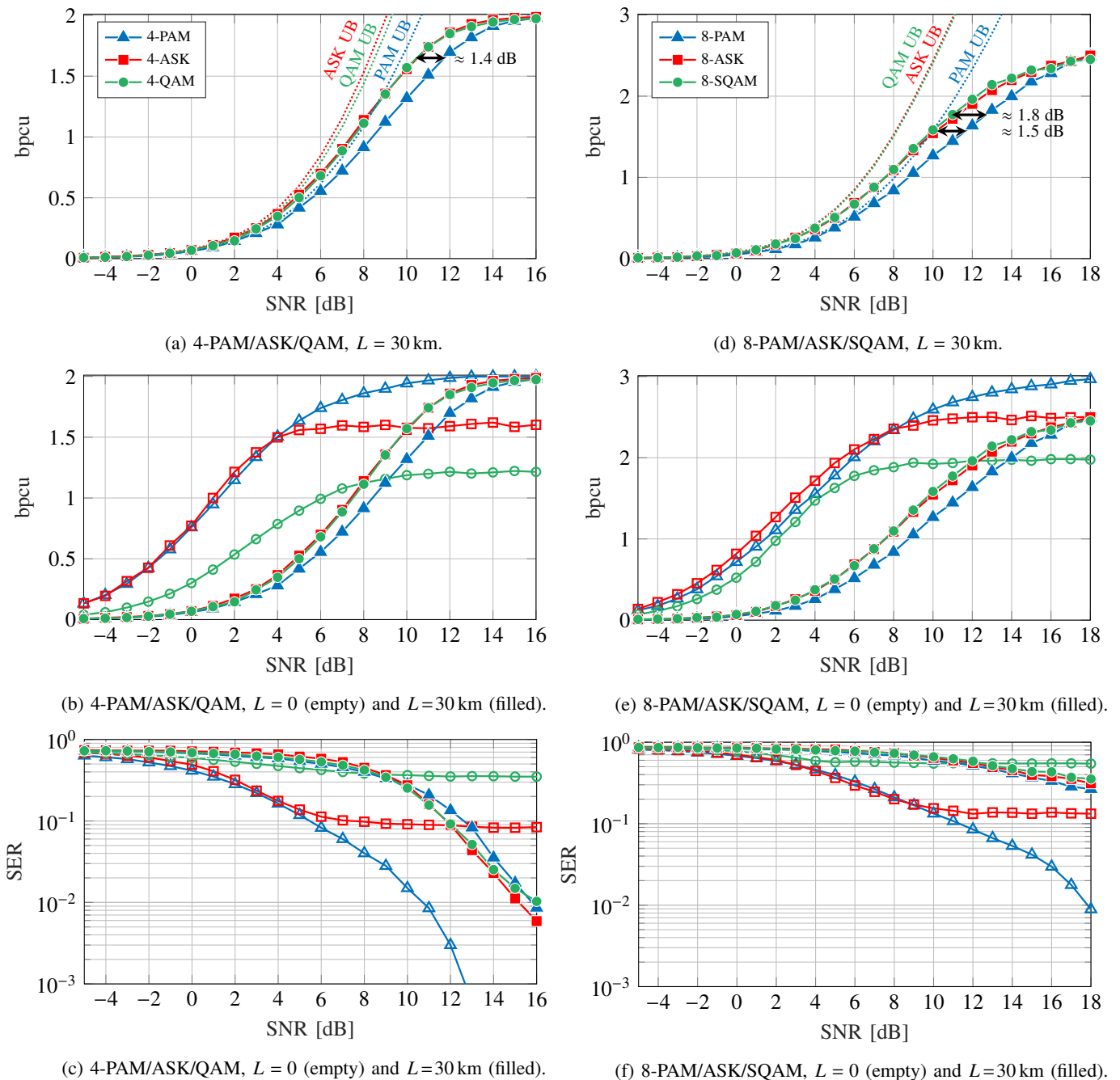


Fig. 8: Achievable rates, upper bounds and HD SERs for $L = 0$ and $L = 30$ km. The auxiliary channel memory is $\tilde{N} = 9$ and $\tilde{N} = 7$ for $Q = 4$ and $Q = 8$, respectively.

APPENDIX

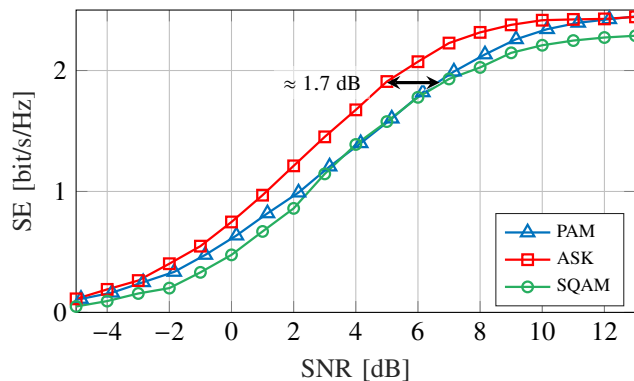
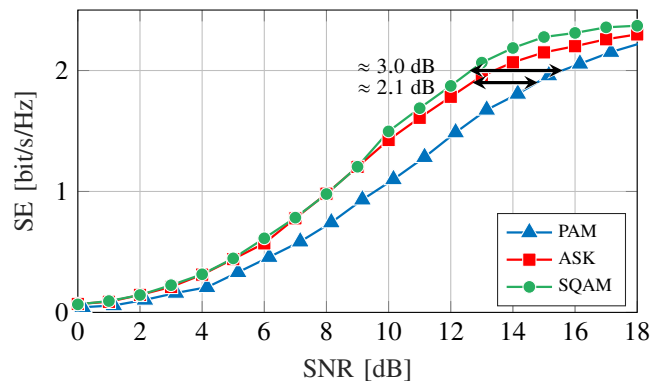
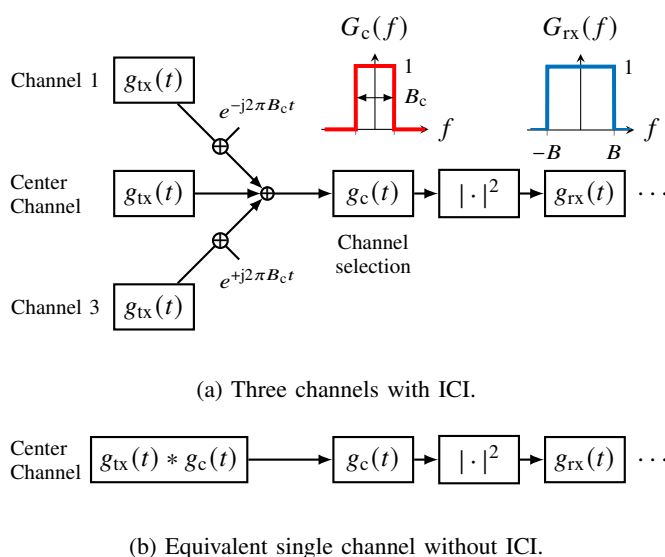
This appendix shows how to minimize the divergence $D(p_{\mathbf{X}\mathbf{Y}} \| p_{\mathbf{X}} \cdot q_{\mathbf{Y}|\mathbf{X}})$ specified in Sec. III-C. Consider the auxiliary channel $q(\mathbf{y}|\mathbf{x}) = \mathcal{N}(\mathbf{y} - |\Psi'\tilde{\mathbf{x}}'|^{\circ 2}; \mu_{\mathbf{Q}}, \mathbf{C}_{\mathbf{Q}\mathbf{Q}})$ and define the interference-plus-noise signal

$$\mathbf{w} = \mathbf{y} - |\Psi'\tilde{\mathbf{x}}'|^{\circ 2} \quad (61)$$

where $\tilde{\mathbf{x}}'$ is an oversampled vector that is extended by the initial channel state \mathbf{s}_0 as in (20). Observe that $\tilde{\mathbf{x}}'$ is a function

of \mathbf{x} and \mathbf{s}_0 . The optimization problem we wish to solve is

$$\begin{aligned} & \arg \min_{\mu_{\mathbf{Q}}, \mathbf{C}_{\mathbf{Q}\mathbf{Q}}} D(p_{\mathbf{X}\mathbf{Y}} \| p_{\mathbf{X}} \cdot q_{\mathbf{Y}|\mathbf{X}}) \\ &= \arg \min_{\mu_{\mathbf{Q}}, \mathbf{C}_{\mathbf{Q}\mathbf{Q}}} \mathbb{E}[-\log_2 q(\mathbf{Y}|\mathbf{X})] \\ &= \arg \min_{\mu_{\mathbf{Q}}, \mathbf{C}_{\mathbf{Q}\mathbf{Q}}} \ln \det \mathbf{C}_{\mathbf{Q}\mathbf{Q}} + \text{tr} \left(\mathbf{C}_{\mathbf{Q}\mathbf{Q}}^{-1} \mathbb{E}[(\mathbf{W} - \mu_{\mathbf{Q}})(\mathbf{W} - \mu_{\mathbf{Q}})^T] \right). \end{aligned}$$

(a) SE for $L = 0$.(b) SE for $L = 30$ km.Fig. 9: SEs for $Q = 8$ and FD-RC pulses with roll-off $\alpha = 0.2$. The auxiliary channel memory is $\tilde{N} = 7$.

(a) Three channels with ICI.

(b) Equivalent single channel without ICI.

Fig. 10: WDM for $L = 0$. The noise is neglected here.

Taking derivatives with respect to μ_Q and C_{QQ} , and setting them to zero, we obtain

$$\mu_Q = \mathbb{E}[\mathbf{W}], \quad C_{QQ} = \mathbb{E}[(\mathbf{W} - \mu_Q)(\mathbf{W} - \mu_Q)^T]. \quad (62)$$

REFERENCES

- [1] M. Chagnon, "Optical communications for short reach," *J. Lightw. Technol.*, vol. 37, no. 8, pp. 1779–1797, April 2019.
- [2] K. Zhong, X. Zhou, J. Huo, C. Yu, C. Lu, and A. P. T. Lau, "Digital signal processing for short-reach optical communications: A review of current technologies and future trends," *J. Lightw. Technol.*, vol. 36, no. 2, pp. 377–400, 2018.
- [3] Q. Hu, M. Chagnon, K. Schuh, F. Buchali, and H. Bülow, "IM/DD beyond bandwidth limitation for data center optical interconnects," *J. Lightw. Technol.*, vol. 37, no. 19, pp. 4940–4946, 2019.
- [4] G. Kramer, A. Ashikhmin, A. van Wijngaarden, and X. Wei, "Spectral efficiency of coded phase-shift keying for fiber-optic communication," *J. Lightw. Technol.*, vol. 21, no. 10, pp. 2438–2445, 2003.
- [5] S. Randel, D. Piloni, S. Chandrasekhar, G. Raybon, and P. Winzer, "100-Gb/s discrete-multitone transmission over 80-km SSMF using single-sideband modulation with novel interference-cancellation scheme," in *Eur. Conf. Optical Commun. (ECOC)*, 2015, pp. 1–3.
- [6] D. Plabst, F. J. García-Gómez, T. Wiegart, and N. Hanik, "Wiener filter for short-reach fiber-optic links," *IEEE Commun. Lett.*, vol. 24, no. 11, pp. 2546–2550, 2020.
- [7] S. D. Dissanayake and J. Armstrong, "Comparison of ACO-OFDM, DCO-OFDM and ADO-OFDM in IM/DD systems," *J. Lightw. Technol.*, vol. 31, no. 7, pp. 1063–1072, 2013.
- [8] L. Chen, B. Krongold, and J. Evans, "Performance analysis for optical OFDM transmission in short-range IM/DD systems," *J. Lightw. Technol.*, vol. 30, no. 7, pp. 974–983, 2012.
- [9] A. Mecozzi and M. Shtaif, "On the capacity of intensity modulated systems using optical amplifiers," *IEEE Photon. Technol. Lett.*, vol. 13, no. 9, pp. 1029–1031, 2001.
- [10] T. Wettlin, S. Calabrò, T. Rahman, J. Wei, N. Stojanovic, and S. Pachnicke, "DSP for high-speed short-reach IM/DD systems using PAM," *J. Lightw. Technol.*, vol. 38, no. 24, pp. 6771–6778, 2020.
- [11] B. Karanov, M. Chagnon, F. Thouin, T. A. Eriksson, H. Bülow, D. Lavery, P. Bayvel, and L. Schmalen, "End-to-end deep learning of optical fiber communications," *J. Lightw. Technol.*, vol. 36, no. 20, pp. 4843–4855, 2018.
- [12] A. Mecozzi and M. Shtaif, "Information capacity of direct detection optical transmission systems," *J. Lightw. Technol.*, vol. 36, no. 3, pp. 689–694, 2018.
- [13] M. Secondini and E. Forestieri, "Direct detection of bipolar pulse amplitude modulation," *J. Lightw. Technol.*, vol. 38, no. 21, pp. 5981–5990, 2020.
- [14] A. Tasbihi and F. R. Kschischang, "On the capacity of waveform channels under square-law detection of time-limited signals," *IEEE Trans. Inf. Theory*, vol. 66, no. 11, pp. 6682–6687, 2020.
- [15] —, "Direct detection under Tukey signalling," *J. Lightw. Technol.*, pp. 1–1, 2021.
- [16] A. Mecozzi, C. Antonelli, and M. Shtaif, "Kramers–Kronig coherent receiver," *Optica*, vol. 3, no. 11, pp. 1220–1227, Nov 2016.
- [17] T. Bo and H. Kim, "Toward practical Kramers-Kronig receiver: Resampling, performance, and implementation," *J. Lightw. Technol.*, vol. 37, no. 2, pp. 461–469, 2019.
- [18] Z. Li, M. Erkilinc, K. Shi, E. Sillekens, L. Galdino, B. Thomsen, P. Bayvel, and R. Killey, "Joint optimisation of resampling rate and carrier-to-signal power ratio in direct-detection Kramers-Kronig receivers," in *Eur. Conf. Optical Commun. (ECOC)*, 2017, pp. 1–3.
- [19] D. Slepian and H. O. Pollak, "Prolate spheroidal wave functions, Fourier analysis and uncertainty — I," *Bell Sys. Techn. J.*, vol. 40, no. 1, pp. 43–63, 1961.
- [20] H. J. Landau and H. O. Pollak, "Prolate spheroidal wave functions, Fourier analysis and uncertainty — II," *Bell Sys. Techn. J.*, vol. 40, no. 1, pp. 65–84, 1961.
- [21] R. Gallager, *Principles of Digital Communication*. Cambridge University Press, 2008.
- [22] R. McEliece and R. Palanki, "Intersymbol interference in pulse-amplitude modulation signaling systems satisfying a spectral mask constraint," The Interplanetary Network Progress Report, IPN PR 42-150, pp. 1–14, April-June 2002.
- [23] A. Lender, "Correlative level coding for binary-data transmission," *IEEE Spectrum*, vol. 3, no. 2, pp. 104–115, 1966.

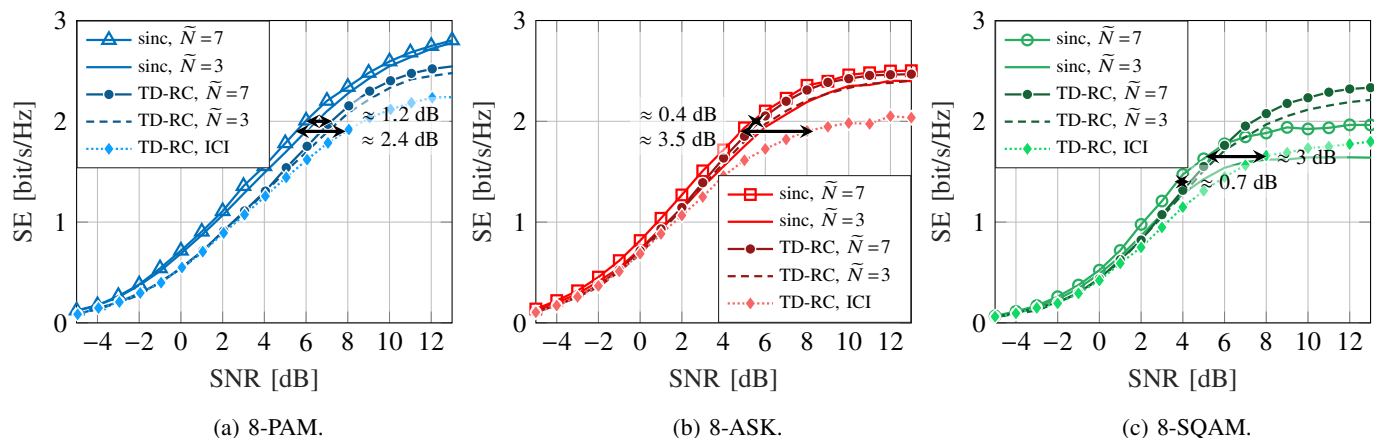


Fig. 11: SEs for $L = 0$, $Q = 8$, a sinc pulse and a TD-RC pulse.

- [24] P. Kabal and S. Pasupathy, "Partial-response signaling," *IEEE Trans. Commun.*, vol. 23, no. 9, pp. 921–934, Sep. 1975.
- [25] L. A. MacColl, "Signaling method and apparatus," United States Patent No. 2,056,284, Oct. 1936.
- [26] A. Lender, "The duobinary technique for high-speed data transmission," *IEEE Trans. Commun. and Electr.*, vol. 82, no. 2, pp. 214–218, 1963.
- [27] J. E. Mazo, "Faster-than-Nyquist signaling," *Bell Sys. Techn. J.*, vol. 54, no. 8, pp. 1451–1462, 1975.
- [28] T. Aulin and C. Sundberg, "Continuous phase modulation - Part I: Full response signaling," *IEEE Trans. Commun.*, vol. 29, no. 3, pp. 196–209, 1981.
- [29] T. Aulin, N. Rydbeck, and C.-E. Sundberg, "Continuous phase modulation - Part II: Partial response signaling," *IEEE Trans. Commun.*, vol. 29, no. 3, pp. 210–225, 1981.
- [30] J. L. Massey, "The how and why of channel coding," in *Int. Zurich Seminar*, 1984, pp. 67–73.
- [31] D. Penninckx, M. Chbat, L. Pierre, and J.-P. Thiery, "The phase-shaped binary transmission (PSBT): a new technique to transmit far beyond the chromatic dispersion limit," *IEEE Phot. Technol. Lett.*, vol. 9, no. 2, pp. 259–261, 1997.
- [32] J. Stark, J. Mazo, and R. Laroia, "Line coding for dispersion tolerance and spectral efficiency: duobinary and beyond," in *Optical Fiber Commun. Conf.*, vol. 2, 1999, pp. 331–333 vol.2.
- [33] E. Forestieri and G. Prati, "Novel optical line codes tolerant to fiber chromatic dispersion," *J. Lightw. Technol.*, vol. 19, no. 11, pp. 1675–1684, 2001.
- [34] E. Forestieri, M. Secondini, F. Fresi, G. Meloni, L. Potí, and F. Cavaliere, "Extending the reach of short-reach optical interconnects with DSP-free direct detection," *J. Lightw. Technol.*, vol. 35, no. 15, pp. 3174–3181, 2017.
- [35] M. Morsy-Osman, F. Fresi, E. Forestieri, M. Secondini, L. Potí, F. Cavaliere, S. Lessard, and D. V. Plant, "50 Gb/s short-reach interconnects with DSP-free direct-detection enabled by CAPS codes," *Opt. Express*, vol. 26, no. 14, pp. 17916–17926, Jul 2018.
- [36] G. Agrawal, *Fiber-Optic Communication Systems*, 4th ed. John Wiley & Sons, Inc., Hoboken, NJ, USA, 2010.
- [37] F. Topsøe, "An information theoretical identity and a problem involving capacity," *Stud. Sci. Math. Hungar.*, vol. 2, pp. 291–292, 1967.
- [38] D. M. Arnold, H.-A. Loeliger, P. O. Vontobel, A. Kavcic, and W. Zeng, "Simulation-based computation of information rates for channels with memory," *IEEE Trans. Inf. Theory*, vol. 52, no. 8, pp. 3498–3508, 2006.
- [39] L. Bahl, J. Cocke, F. Jelinek, and J. Raviv, "Optimal decoding of linear codes for minimizing symbol error rate," *IEEE Trans. Inf. Theory*, vol. 20, no. 2, pp. 284–287, 1974.
- [40] T. M. Cover and J. A. Thomas, *Elements of Information Theory*, 2nd ed. John Wiley & Sons, Inc., Hoboken, NJ, USA, 2006.
- [41] R.-J. Essiambre, G. Kramer, P. J. Winzer, G. J. Foschini, and B. Goebel, "Capacity limits of optical fiber networks," *J. Lightw. Technol.*, vol. 28, no. 4, pp. 662–701, 2010.
- [42] H. Pfister, J. Soriaga, and P. Siegel, "On the achievable information rates of finite state ISI channels," in *IEEE Global Telecommun. Conf.*, vol. 5, 2001, pp. 2992–2996 vol.5.
- [43] C. E. Shannon, "A mathematical theory of communication," *Bell Sys. Techn. J.*, vol. 27, pp. 379–423 and 623–656, July and October 1948, Reprinted in *Claude Elwood Shannon: Collected Papers*, pp. 5–83, (N.J.A. Sloane and A.D. Wyner, eds.) Piscataway: IEEE Press, 1993.
- [44] F. Steiner, "Coding for higher-order modulation and probabilistic shaping," Dissertation, Fakultät für Elektrotechnik und Informationstechnik, Technische Universität München, München, 2020.
- [45] K. Jaganathan, S. Oymak, and B. Hassibi, "Sparse phase retrieval: Convex algorithms and limitations," in *IEEE Int. Symp. Inf. Theory*, 2013, pp. 1022–1026.
- [46] H. Qiao and P. Pal, "Sparse phase retrieval with near minimal measurements: A structured sampling based approach," in *IEEE Int. Conf. Acoustics, Speech and Signal Proc. (ICASSP)*, 2016, pp. 4722–4726.
- [47] P. Schniter and S. Rangan, "Compressive phase retrieval via generalized approximate message passing," *IEEE Trans. Signal Process.*, vol. 63, no. 4, pp. 1043–1055, 2015.
- [48] W. Weber, "Differential encoding for multiple amplitude and phase shift keying systems," *IEEE Trans. Commun.*, vol. 26, no. 3, pp. 385–391, 1978.
- [49] P. Hoehner and J. Lodge, "'turbo DPSK': Iterative differential PSK demodulation and channel decoding," *IEEE Trans. Commun.*, vol. 47, no. 6, pp. 837–843, 1999.
- [50] L. Schmalen, S. ten Brink, and A. Leven, "Advances in detection and error correction for coherent optical communications: Regular, irregular, and spatially coupled LDPC code designs," *CoRR*, vol. abs/1704.04618, 2017. [Online]. Available: <http://arxiv.org/abs/1704.04618>
- [51] S. Howard and C. Schlegel, "Differential turbo-coded modulation with APP channel estimation," *IEEE Trans. Commun.*, vol. 54, no. 8, pp. 1397–1406, 2006.